Proceedings of the ASME Turbo Expo 2024
Turbomachinery Technical Conference and Exposition
GT2024
June 24–28, 2024, London, England, United Kingdom

GT2024-123859

A COMPARISON OF MODEL PREDICTIVE CONTROL ARCHITECTURES FOR APPLICATION TO ELECTRIFIED AIRCRAFT PROPULSION SYSTEMS

Elyse D. Hill[1,*], Donald L. Simon[2,*], Joseph W. Connolly[3]

[1]NASA Postdoctoral Program Fellow, Oak Ridge Associated Universities, Oak Ridge, TN
[2]Control Systems Engineer, NASA Glenn Research Center, Cleveland, OH
[3]Project Integration Lead, NASA Glenn Research Center, Cleveland, OH

ABSTRACT

As electrified aircraft propulsion (EAP) systems continue to mature, more sophisticated hardware and software are being developed to balance operations among electric machines and gas-turbine engines. In hybrid-electric propulsion systems, the increased complexity resulting from integrating turbine-engine shafts with electric machines necessitates control methodologies to account for various physical domains. Ideal controllers for hybrid-electric engines manage systems, subsystems, and their interactions in a coordinated fashion, able to account for safety and performance goals while being computationally efficient. In a previous work, linear model predictive control (MPC) schemes were implemented in centralized and distributed frameworks on a nonlinear turbofan engine model as a proof of concept. However, these schemes were not evaluated for computational complexity, prompting further study. The research presented here develops hierarchical MPC schemes to reduce the computational burden of the previous MPC schemes. A two-tier framework is implemented, where a slower sampling MPC controls electric machines and determines fan-speed tracking goals for a faster sampling controller, which is either a MPC or a proportional-integral (PI) controller. The proposed designs are compared to the centralized MPC investigated previously, and performance is measured via fan speed tracking error, energy storage state-of-charge, and computation time. Results reveal that the hierarchical MPC scheme employing a lower-level PI controller improves computation time while maintaining comparable tracking and state-of-charge regulation to the centralized scheme.

Keywords: model predictive control, linear control, hierarchical control, turbomachinery, electrified aircraft propulsion

NOMENCLATURE

Roman letters

A	System state matrix.
a	Washout filter variable for exponential decay.
B	System input matrix.
C	System output matrix.
C_{SC}	Capacitance of supercapacitor.
D	System feedforward matrix.
e	Error variable.
E	Supercapacitor state-of-charge.
J	Open-loop cost function.
K	Gain value for proportional-integral controller.
l	Stage cost function.
M	Motor torque variable.
m	Number of control inputs.
N	Shaft speed variable.
P_{s3}	Static high pressure compressor discharge pressure.
Q	Output weight matrix.
r	Number of outputs.
R	Control weight matrix.
SM	Stall margin.
t	Simulation time.
T, T_u	Time horizon, time horizon for inputs variables.
T_s	Sampling time.
T_{45}	Low pressure turbine inlet temperature.
u	System control input.
$\mathcal{U}$	System control constraint set.
V	Voltage.
VAFN	Variable area fan nozzle variable.
VBV	Variable bleed valve variable.
W_f	Fuel flow rate variable.
x	System states.
$\mathcal{X}$	System state constraint set.
y	System outputs.
$\mathcal{Y}, \mathcal{Y}_f$	System output constraint and terminal constraint set.

Greek letters

*Corresponding author: elyse.d.hill@nasa.gov, donald.l.simon@nasa.gov

α Sampling time multiplier.
Δ Change between time steps.
δ System perturbation variable.
η Energy efficiency variable.
ν Prediction horizon variable.
Ω Augmented input vector.
ϕ Acceleration threshold value.
τ Time sequence over time horizon.

Superscripts and subscripts

$\cdot^*$ Denotes optimal solution.
$\cdot_0$ Denotes initial variable value.
$\cdot_{aug}$ Denotes augmented vector.
$\cdot_c$ Denotes corrected speed variable.
$\cdot_E$ Denotes relation to energy storage.
$\cdot_f$ Denotes relation to fuel.
$\cdot_{fan}$ Denotes relation to fan variable.
$\cdot_{HPC}$ Denotes relation to high pressure compressor.
$\cdot_{HPS}$ Denotes relation to high pressure shaft.
$\cdot_i$ Denotes index placeholder.
$\cdot_I$ Denotes relation to integral error value.
$\cdot_{LPC}$ Denotes relation to low pressure compressor.
$\cdot_{LPS}$ Denotes relation to low pressure shaft.
$\cdot_{max}$ Denotes maximum value.
$\cdot_{norm}$ Denotes normalized variable.
$\cdot_P$ Denotes relation to proportional error value.
$\cdot_{ref}$ Denotes reference parameter variable.
$\cdot_{SC}$ Denotes relation to supercapacitor.
$\cdot_{SS}$ Denotes operation at engine steady-state.
$\cdot_{trim}$ Denotes trim value.
$\tilde{\cdot}$ Denotes error.
$\cdot_{washout}$ Denotes relation to washout filter.

1. INTRODUCTION

Under goals outlined by NASA's Aeronautics Research Mission Directorate, sustainability and safety are drivers for current and future aeronautics research [1]. This has increased focus on the electrification of aviation technology, which includes the development and testing of electrified aircraft propulsion (EAP) systems. A result of integrating, supplementing, or replacing traditional gas-turbine based propulsors with electric components is heightened system complexity due to coupled system dynamics [2]. Thus, the sophisticated nature of EAP begets the need for advanced control architectures to manage the increasingly interconnected systems [3].

Recent studies have considered model predictive control (MPC) as a viable approach to controlling EAP systems [4–10]. MPC is an advanced, model-based control method that determines an optimal control effort along a time horizon for a dynamic system while adhering to imposed constraints [11]. Widely applied in the process control industry, MPC is known for its ability to control complex, multivariable systems while balancing multiple system goals. This makes the method attractive for EAP systems, as it can command the coupled components and their interactions in a holistic and beneficial manner. This was highlighted in a recent work in which centralized and distributed MPC architectures were introduced for control of a hybrid-electric EAP system [12]. The proposed controllers implemented the Turbine Electrified Energy Management (TEEM) concept to improve transient operability by exploiting electric machines during system acceleration and deceleration. While shown comparable to a baseline control scheme, these architectures did not consider energy storage components and thus included no battery state-of-charge regulation.

Although effective, a common pitfall of traditional MPC schemes is their computational intensity, requiring significant computing time to determine an optimal solution [13]. A source of this computing strain is the use of one sampling frequency which scales with system complexity given horizon time and number of decision variables. As a result, methods to reduce computational burden while maintaining system performance are warranted. To combat the computational load of MPC, hierarchical MPC (HMPC) has been proposed, in which an MPC acts in a supervisory manner to oversee system and subsystem controllers at various layers or tiers to address goals and constraints [14]. By managing the system in tiers, the overall control architecture can incorporate multiple timescales and reduce control problem complexity [15, 16]. This approach helps to decrease the computational footprint of centralized, distributed, or decentralized MPC schemes that scale with system complexity, time horizon duration, and sampling frequency. HMPC has precedent in EAP system applications where energy, power, and thermal management were examined [17–21].

In this paper, two linear HMPC schemes are developed in which a supervisory centralized MPC (CMPC) is used to set optimal setpoints for a lower-level controller. The lower-level controller is either another CMPC or a proportional-integral (PI) controller, resulting in a MPC-MPC or MPC-PI hierarchy. The supervisory CMPC operates at a slower sampling speed while the lower-tier controllers operate at the sampling rate of the plant. The supervisory control for the HMPCs expands on the framework developed in [12] by including energy storage components. The controllers are simulated on a nonlinear, hybrid-electric engine system for performance comparison to a CMPC based on closed-loop performance and algorithm execution times.

The remainder of this manuscript is organized as follows: Section 2 reviews the nonlinear engine system, its linear representation, and a previous MPC implementation. The hierarchical MPC architectures are detailed in Section 3, followed by a discussion of simulated case study results in Section 4. Finally, the primary conclusions of the study are summarized in Section 5.

2. OVERVIEW OF ENGINE MODEL AND TEEM

2.1 System Model

This section details an electrified version of the Advanced Geared Turbofan 30,000lbf (AGTF30) engine, the dynamic system of interest. Figure 1 displays a generalized block diagram of the closed-loop control system for the propulsion system, where a controller receives environmental information and provides output commands to the engine and electric machine (EM) actuators. The AGTF30 is a conceptual turbofan engine capable of producing 30klbf of thrust at sea-level static conditions [22]. The engine was developed with the Toolbox for the Modeling and Analysis of Thermodynamic Systems in the MATLAB/Simulink environment. Electrification was added in [23], integrating components

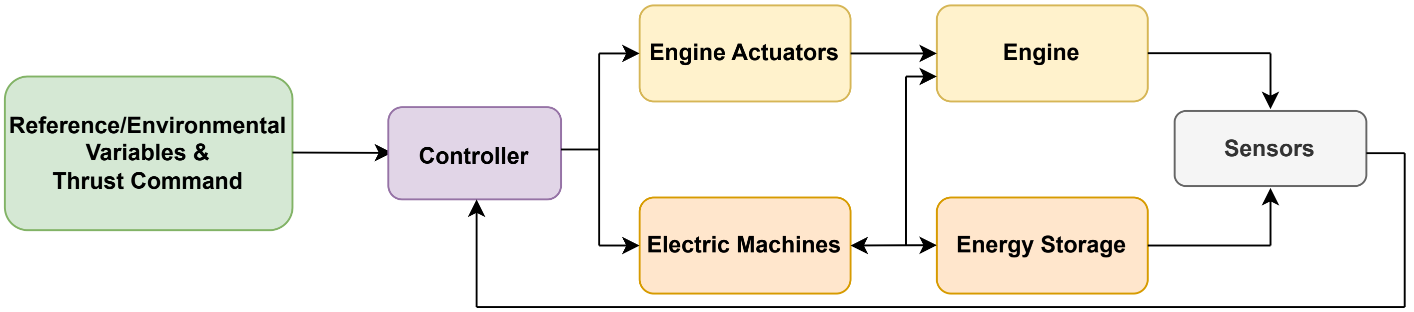

FIGURE 1: GENERALIZED BLOCK DIAGRAM OF THE SYSTEM.

from the Electrical Modeling and Thermal Analysis Toolbox [24] to include electric machines and energy storage devices (ESDs). In this study, two electric machines are coupled to the engine, with one EM connected to the low pressure spool (LPS) and the other to the high pressure spool (HPS).

In the literature, the EMs are used to implement the TEEM concept by injecting or extracting power from the engine shafts during acceleration and deceleration transients [25]. Note that although TEEM is implemented in this work, the focus of the paper will be on comparing the MPC architectures rather than the TEEM operability outcomes. Power extraction can be used to charge the ESDs, which are supercapacitors responsible for absorbing and supplying impulsive power loads during transients. The EMs responsible for this task can vary depending on the configurations outlined in [26]. This study considers a variant of the dual-spool configuration, in which the LPS EM is responsible for charging the ESDs using power extraction. Any excess power that cannot be transferred to the ESD is dissipated with a resistor bank to prevent overcharging the supercapacitors.

For control design purposes, a piece-wise linear model is used to represent the nonlinear dynamics of the propulsion system:

$$\delta\dot{x}(t) = A\delta x(t) + B\delta u(t) \tag{1}$$
$$\delta y(t) = C\delta x(t) + D\delta u(t) \tag{2}$$

where $x(t) \in \mathbb{R}^n$ is the state vector, $u(t) \in \mathbb{R}^m$ is the input vector, $y(t) \in \mathbb{R}^r$ is the output vector, and A, B, C and D are the dynamic system state space matrices. The model is linearized at specific operating points denoted by combinations of altitude (Alt), and Mach number (MN), and the power lever angle (PLA) of the throttle command. The terms $\delta x, \delta u$, and δy represent perturbations around the value of the state, input, or output vectors at engine steady-state, denoted with the subscript $\cdot_{trim}$, and are defined as:

$$\delta x(t) = x(t) - x_{trim}(t) \tag{3a}$$
$$\delta u(t) = u(t) - u_{trim}(t) \tag{3b}$$
$$\delta y(t) = y(t) - y_{trim}(t) \tag{3c}$$

The dynamic equation for the ESDs with time argument t omitted is:

$$\dot{E} = \eta[-(M_{LPS}N_{LPS}) - (M_{HPS}N_{HPS})] \tag{4}$$

where E represents the energy of the supercapacitor, η represents an efficiency term, N_{LPS} and N_{HPS} are the LPS and HPS speeds, and M_{LPS} and M_{HPS} are the motor torques of the electric machines on the low and high pressure shafts. Equation 4 is a linear approximation of energy used by the EMs in the nonlinear propulsion system, encapsulating contributions from the electric machines, power electronics, ESDs, and other elements in the electric powertrain. Further, the sign conventions used in Eq. 4 indicate the impact of the EMs on the state-of-charge. M_{LPS} produces negative torque via power extraction and is leveraged to charge the ESD. M_{HPS} produces positive torque via power injection and depletes the ESD.

The states, inputs, and outputs for the propulsion system in this work are:

$$\begin{aligned} x_{aug} &= \begin{bmatrix} N_{LPS} & N_{HPS} & E \end{bmatrix}^T \\ &= \begin{bmatrix} x & E \end{bmatrix}^T \end{aligned} \tag{5}$$
$$u = \begin{bmatrix} W_f & M_{LPS} & M_{HPS} & VAFN & VBV \end{bmatrix}^T \tag{6}$$
$$y = \begin{bmatrix} P_{s3} & T_{45} & N_{fan} & N_{HPS} \end{bmatrix}^T \tag{7}$$

Equation 5 is an augmented state vector stacking the LPS and HPS speeds with the ESD state-of-charge. The inputs in Eq. 6 include the fuel flow rate, LPS and HPS electric machine torques, variable area fan nozzle (VAFN) area, and variable bleed valve (VBV) setting. Equation 7 denotes the static high pressure compressor discharge pressure, the low pressure turbine inlet temperature, the uncorrected fan speed, and the uncorrected high pressure shaft speed. Note fan speed is used as a proxy for thrust and is related to the LPS speed by a gear ratio expressed as $N_{LPS} = 3.1N_{fan}$ for the given propulsion system.

2.2 MPC Implementation

Previously, Ref. [12] proposed a CMPC formulation for the AGTF30 system with the following optimal control problem:

Problem 1 (Centralized MPC Optimal Control Problem)

$$\min_{u} \quad J(\delta y, \delta u) \tag{8a}$$
$$\textit{subject to} \quad \delta y(t) = \delta y_0 \tag{8b}$$
$$\delta\dot{x}(\tau) = A\delta x(\tau) + B\delta\Omega(\tau), \tag{8c}$$
$$\delta y(\tau) = C\delta x(\tau) + D\delta\Omega(\tau), \tag{8d}$$
$$\delta x(\tau) \in \mathcal{X} - x_{trim}, \tag{8e}$$

$$\delta\Omega(\tau) \in \mathcal{U} - u_{trim}, \quad (8f)$$
$$\delta y(\tau) \in \mathcal{Y} - y_{trim}, \quad (8g)$$
$$\delta y(t+T) \in \mathcal{Y}_f - y_{trim}, \quad (8h)$$
$$\tau \in [t, t+T]$$

where the open-loop cost function is:

$$J(\delta y, \delta u) = \int_t^{t+T} l(\delta\tilde{y}(\tau))d\tau + \int_t^{t+T_u} l(\Delta u(\tau), \delta u_{washout}(\tau))d\tau \quad (9)$$

and where T, T_u are the time horizons for the outputs and inputs respectively with $T_u \le T$. In Problem 1, τ is the time variable over the horizon, y_0 is the initial condition of the output, and $\mathcal{X}, \mathcal{U}, \mathcal{Y}$, and $\mathcal{Y}_f$ are the state, input, output, and terminal constraint sets, respectively. The term Ω is an input vector described as:

$$\Omega(\tau) = \begin{bmatrix} W_f(\tau) & M_{LPS}(\tau) & M_{HPS}(\tau) & VAFN(t) & VBV(t) \end{bmatrix}^T \quad (10)$$

Ω combines the decision variables as a function of the horizon τ and the open-loop scheduled inputs as a function of the initial time instant t. The stage costs $l(\cdot)$ are quadratic and represented by the weighted Euclidean norm $\|\cdot\|_\Pi^2$ with symmetric, positive-definite weighting matrix Π. The stage costs in Eq. 9 are:

$$l(\delta\tilde{y}(\tau)) = \|\delta\tilde{y}\|_Q^2 \quad (11)$$
$$l(\Delta u(\tau), \delta u_{washout}(\tau)) = \|\Delta u\|_R^2 + \|\delta u_{washout}\|_{R_{washout}}^2 \quad (12)$$

where Q, R, and $R_{washout}$ are weighting matrices. The components of the stage costs include:

$$\tilde{y} = \begin{bmatrix} \tilde{y}_{1,1} = & N_{fan} - N_{fan,ref} \\ \tilde{y}_{2,1} = & \begin{cases} N_{LPS} - N_{LPS,SS} & if \quad \dot{N}_{fan} < -\phi \\ N_{HPS} - N_{HPS,SS} & if \quad \dot{N}_{fan} > \phi \\ 0 & otherwise \end{cases} \end{bmatrix} \quad (13)$$

$$\Delta u = \delta u(\tau) - \delta u(\tau - T_s) \quad (14)$$
$$u_{washout} = (-ae^{-at})^{-1} \begin{bmatrix} M_{LPS} & M_{HPS} \end{bmatrix} \quad (15)$$

where the subscript $\cdot_{SS}$ represents a steady-state value, $\dot{N}_{fan}$ is fan acceleration, ϕ is a threshold value, $a \ge 0$ is a non-negative value, and T_s is the sampling time. The piecewise logic in Eq. 13 permits only one steady-state setpoint to be tracked in $\tilde{y}$ at a time, with the LPS setpoint tracked during deceleration and the HPS setpoint tracked during acceleration in accordance with the TEEM strategy. These setpoints are not tracked during steady-state operation, indicated by the *otherwise* condition. The output of Problem 1 is the optimal open-loop control sequence over the time horizon $u^*(\cdot; x(t))$, where $\cdot^*$ denotes the optimal solution. This is accompanied by the resultant optimal state trajectory, $x^*(\cdot; x(t), u^*(\cdot; x(t)))$.

Under the dual-spool configuration, M_{LPS} in Eq. 4 is responsible for charging the ESDs. As opposed to the prior implementation in [12], the LPS EM is now permitted to activate during steady-state operation to charge the supercapacitor. While activated at steady-state, M_{LPS} does not engage in the tracking goal outlined in $\tilde{y}_{2,1}$ as that goal is restricted to deceleration transients. To permit charging of energy storage devices, an additional stage cost is added to Eq. 9. This stage cost includes a penalty on an inverted washout filter term to regulate E to a setpoint E_{ref} during engine steady-state conditions:

$$\|(-a_E(E_{ref} + e^{-a_E t})^{-1} E\|_{Q_E}^2 \quad (16)$$

where the values $a_E \ge 0$ and Q_E control the speed and magnitude of the response. To restrict, but not necessarily eliminate, potential overcharging, a term is used to penalize LPS EM activation in instances where $E \ge E_{ref}$:

$$\|M_{LPS}\|_{R_E}^2 \quad (17)$$

Combining Eqs. 16 and 17 into a stage cost using piecewise logic forms:

$$l(\delta x_{aug}, \delta u) = \begin{cases} \|M_{LPS}\|_{R_E}^2 & if \quad E \ge E_{ref} \\ \|(-a_E(E_{ref} + e^{-a_E t})^{-1} E\|_{Q_E}^2 & otherwise \end{cases} \quad (18)$$

The updated CMPC optimal control problem now reads as:

Problem 2 (Updated CMPC Optimal Control Problem)

$$\min_u \quad J(\delta y, \delta x_{aug}, \delta u) \quad (19a)$$
$$\textit{subject to} \quad \delta y(t) = \delta y_0 \quad (19b)$$
$$E(t) = E_0, \quad (19c)$$
$$\delta\dot{x}(\tau) = A\delta x(\tau) + B\delta\Omega(\tau), \quad (19d)$$
$$\dot{E}(\tau) = f((\delta x(\tau) + x_{trim}), (\delta u(\tau) + u_{2:3,trim})), \quad (19e)$$
$$\delta y(\tau) = C\delta x(\tau) + D\delta\Omega(\tau), \quad (19f)$$
$$\delta x_{aug}(\tau) \in \mathcal{X}_{aug} - x_{aug,trim}, \quad (19g)$$
$$\delta\Omega(\tau) \in \mathcal{U} - u_{trim}, \quad (19h)$$
$$\delta y(\tau) \in \mathcal{Y} - y_{trim}, \quad (19i)$$
$$\delta y(t+T) \in \mathcal{Y}_f - y_{trim}, \quad (19j)$$
$$\tau \in [t, t+T]$$

where Eq. 19e is equivalent to Eq. 4 in terms of the perturbation values and the open-loop cost function is:

$$J(\delta y, \delta x_{aug}, \delta u) = \int_t^{t+T} l(\delta\tilde{y}(\tau))d\tau + \int_t^{t+T_u} l(\Delta u(\tau), \delta u_{washout}(\tau))d\tau + \int_t^{t+T} l(\delta x_{aug}(\tau), \delta u(\tau))d\tau \quad (20)$$

3. CONTROLLER DESIGN

This section describes the proposed hierarchical MPC architectures. In HMPC schemes, the top-most controller is an MPC and subsequent tier controllers can be any control scheme. In this paper, a 2-tier, one subsystem layout is considered where

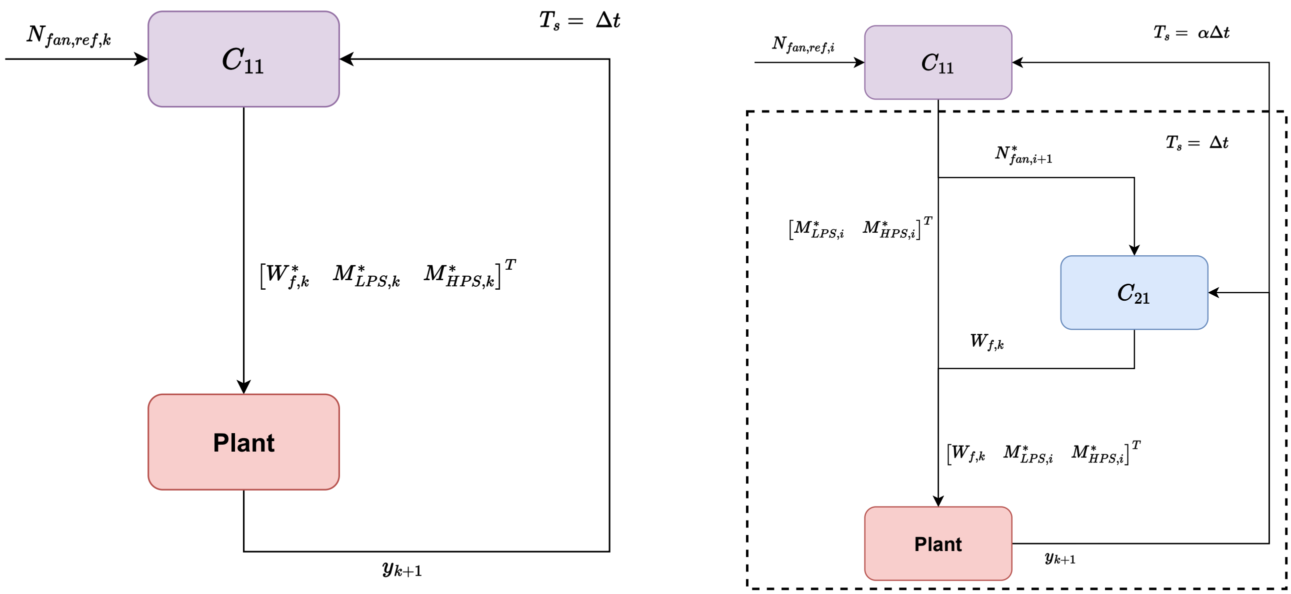

(a) Centralized MPC architecture.

(b) Hierarchical MPC architecture.

FIGURE 2: SIMPLIFIED CENTRALIZED AND HIERARCHICAL MPC ARCHITECTURES.

the highest tier controller (C_{11}) is a CMPC and the lowest tier controller (C_{21}) is a PI controller or another CMPC. These two configurations are referred to as MPC-PI and MPC-MPC, respectively. Figure 2 illustrates the difference between CMPC and HMPC implementations. In Fig. 2a, C_{11} is a CMPC sampled at the discretization rate of the plant, $T_s = \Delta t$, commanding the first instance of the optimal open-loop input sequence to and receiving feedback from the plant. In contrast, the HMPC scheme depicted in Fig. 2b features two sample rates: $T_s = \alpha\Delta t$ for the first tier, indexed with i, and $T_s = \Delta t$ for the second tier, indexed with k. The term α is a positive integer used to alter the sample time at higher tiers. The control C_{11} tracks the reference trajectory and sets the optimal setpoint for C_{21} when the sample times coincide from its resultant optimal state trajectory. The control C_{21} then produces an input to be applied to the plant, whose outputs are sent to C_{21} and C_{11} when the sample rates sync. The propulsion system permits a two-subsystem layout, where one subsystem is actuated by the engine inputs and the second subsystem is actuated by the electric machines. This would result in two second-tier controllers: C_{21} and C_{22}. However, this paper only considers the gas turbine engine components as a subsystem, actuated by the fuel flow rate W_f and controlled by C_{21}. This decision removes the need for C_{22} and results in C_{11} bearing responsibility for determining the remaining active control variables, i.e. the motor torques, depicted in Fig. 2b as communicated to the plant when $i = k$.

The optimal control problem for C_{11} of both the MPC-PI and MPC-MPC architectures is identical to Problem 2. The PI portion of MPC-PI is defined as:

$$u_{PI} = K_P e(t) + K_I \int e(\tau)dt \tag{21}$$

where K_P, K_I are proportional and integral gains. The error is $e = N_{c,fan} - N_{c,fan,ref}$ where the subscript $\cdot_c$ refers to the corrected shaft speed. For details on the PI formulation, refer to [22]. The optimal control problem for the C_{21} portion of the MPC-MPC is identical to Problem 1 but uses a different augmented input and cost function:

$$\Omega = \begin{bmatrix} W_f(\tau) & M_{LPS}(t) & M_{HPS}(t) & VAFN(t) & VBV(t) \end{bmatrix}^T \tag{22}$$

$$J(\delta y, \delta u) = \int_t^{t+T} l(\delta\tilde{y}_{1,1}(\tau))d\tau + \int_t^{t+T_u} l(\Delta u_{W_f}(\tau)) \tag{23}$$

In contrast to Eq. 10, Eq. 22 includes a decision variable, open-loop scheduled variables, and the optimal motor torques M^*_{LPS} and M^*_{HPS} supplied by C_{11}. The stage costs in Eq. 23 use the weight matrices Q_e for the tracking penalty and R_e for the input penalty.

4. CASE STUDIES

The developed controllers are verified on the nonlinear model with a simulated burst-chop transient at sea-level-static conditions (Alt = 0kft, MN = 0) with a PLA change from 48° to 80° to 48°. The simulation time is 65s with the burst starting at 10s and the chop starting at 40s. All controllers are tuned to achieve a five-second rise time across the burst-chop transient and to maintain a normalized supercapacitor state-of-charge above a user-selected value of 90%. Simulations are implemented in MATLAB/Simulink using direct multiple shooting with CasADi for MPC optimization. CasADi includes the nonlinear optimization library iPOPT [27]. The discretization rate is set to $\Delta t = 0.015s$ with $\alpha = 35$ for the MPC-PI and $\alpha = 10$ for the MPC-MPC. Note for CMPC, $T_s = \Delta t$. There is currently no direct guideline for selecting α, however the parameter is often selected based on the speed of the dynamic system and must be manipulated to ensure closed-loop stability [18]. In each controller, the time horizons are set by the relationship $\nu = \frac{T}{T_s}$, with $\nu = 5$ for T and $\nu_u = 2$ for T_u. To account for computational delay, traditionally assumed to be negligible in MPC implementation, the second, rather than first, element in the optimal input sequence is applied to the plant. As a result, C_{21} receives the third element in the optimal state trajectory from C_{11}. Closed-loop performance is evaluated with uncorrected fan speed, normalized supercapacitor state-of-charge, and electric machine data. Further, computation time among the control approaches is compared based on the normalized average block execution and total execution times in Simulink. The normalized state-of-charge is a percentage determined as outlined in [26]:

$$V_{norm} = \frac{V_{SC}}{V_{SC,max}} * 100 \tag{24}$$

where V_{norm} is the normalized voltage, V_{SC} is the voltage across the supercapacitor bank, and $V_{SC,max}$ is the voltage at which the supercapacitor bank is considered to be at full charge. Please note that the value at which the supercapacitor is considered to be at the desired maximum charge is below the maximum voltage capability of the supercapacitor. $V_{SC,max}$ is used to determine the setpoint E_{ref}. The voltage across the supercapacitor bank is related to energy via the relationship $E = 0.5C_{SC}V^2$ where C_{SC} is the capacitance of the supercapacitor. The following constraint sets are used:

$$\begin{aligned}
\mathcal{X}_{aug} = \{&0\text{rpm} \leq N_{LPS} \leq 7130\text{rpm},\\
&0\text{rpm} \leq N_{HPS} \leq 22500\text{rpm},\\
&0\text{J} \leq E \leq 5.4 \times 10^7\text{J}\}\\
\mathcal{Y} = \mathcal{Y}_f = \{&0\text{psi} \leq P_{s3} \leq 790\text{psi}, 0°\text{R} \leq T_{45} \leq 2414°\text{R},\\
&0\text{rpm} \leq N_{fan} \leq 2300\text{rpm},\\
&0\text{rpm} \leq N_{HPS} \leq 22500\text{rpm}\}\\
\mathcal{U} = \{&W_{f,lb}(t)\text{pps} \leq W_f \leq W_{f,ub}(t)\text{pps},\\
&-600\text{ft-lbf} \leq M_{LPS} \leq 0\text{ft-lbf},\\
&0\text{ft-lbf} \leq M_{HPS} \leq 200\text{ft-lbf}\}
\end{aligned}$$

where the subscripts $\cdot_{lb}, \cdot_{ub}$ indicate lower and upper bounds and the fuel flow rate constraints are time-varying functions defined in the engine model. These constraints are based on safety factors related to fan acceleration, shaft speed, pressure, and temperature for the engine system and span the engine's entire flight envelope. The electric motor constraints are selected based on maximum power and torque capabilities for the electrified engine system. Further, their definitions restrict M_{HPS} to power injection during acceleration transients and M_{LPS} to power extraction during deceleration transients and at steady-state. The remainder of the section presents simulation results for the following cases:

1. Performance Comparison of HMPCs to CMPC
2. Effect of Sampling Time on HMPC

4.1 Performance Comparison of HMPCs to CMPC

Figure 3 displays the closed-loop performance of the controllers, with several magnified insets to highlight noticeable outcomes. Further, Fig. 4 presents relevant parameters that are important for engine safety and life maintenance. All controllers meet the fan speed rise requirement, with various degrees of steady-state error present, while not violating critical temperature or stall margin restrictions. In terms of responsiveness, both HMPCs lag the CMPC and have elements of steady-state error and undershoot with respect to the reference signal. Further, the hierarchical controllers diverge slightly from the fan speed reference trajectory prior to burst, as displayed in the inset of the first 10s of the response in Fig. 3. Such an outcome is undesirable, as thrust response is the priority objective of engine control. Subsequent investigation revealed the resultant behavior of the HMPCs to be impacted by α, to be discussed in the next section. However, potential solutions to curb this response include adding an integral term to the cost function or by implementing rate-based MPC, which is known for its ability to mitigate steady-state error. Thus, these options should be explored in future work.

The controllers respond to the state-of-charge tracking goal included in the cost function, resulting in ESD charging during steady-state as shown in the plot of the normalized voltage. Indeed, after actuating M_{HPS} during burst, all controllers begin to charge the ESDs once the system has reached steady-state at high power PLA. Charging continues when M_{LPS} actuates during chop, resulting in sharp voltage depletions in V_{norm} at $t > 40$s across the controllers where the supercapacitors reach full charge and the resistor bank dissipates excess power. The final value of E is static across controllers due to the deactivation of M_{LPS}, causing each controller to hold the state-of-charge at the ending voltage of the resistor bank dissipation. This behavior can be combatted by manipulating the related washout filter variables $(a, R_{washout})$ to permit the motor to be active longer or by manipulating the energy charging variables (a_E, Q_E) to better emphasize the charging objective. Prior to the burst, the state-of-charge appears to diverge slightly from the reference in some controllers, displayed in the magnified inset. The graph of M_{HPS} shows minor actuations on the HPS EM during this time. As actuation of M_{HPS} consumes energy, M_{LPS} activates to restore the energy. For example, the CMPC inadvertently activates the HPS EM at $t < 2$s, forcing the state-of-charge below the setpoint. The state-of-charge soon begins to move towards the setpoint due to activation of M_{LPS} after $t = 2$s. Similar behavior is observed in MPC-PI, where minor fluctuations can be observed on the LPS EM in response to HPS EM actuations. While these responses show that the current logic for state-of-charge tracking is feasible, it also illustrates the stage cost should be refined to remove this behavior. This is especially true as the HPS EM should not be active at steady-state in accordance with the TEEM strategy. Further, although the fluctuating behavior is observed across all controllers, the influence of α on the behavior should be explored in the HMPCs, as the sampling time parameter affects the transient response.

In addition to system performance, computational burden is also used as an evaluation metric. Figure 5 presents normalized average execution times for the controllers relative to the CMPC for both the total Simulink file execution time and the total controller execution time. These values were determined by running ten repeated simulations of each controller, averaging the execution times, and then normalizing the execution times

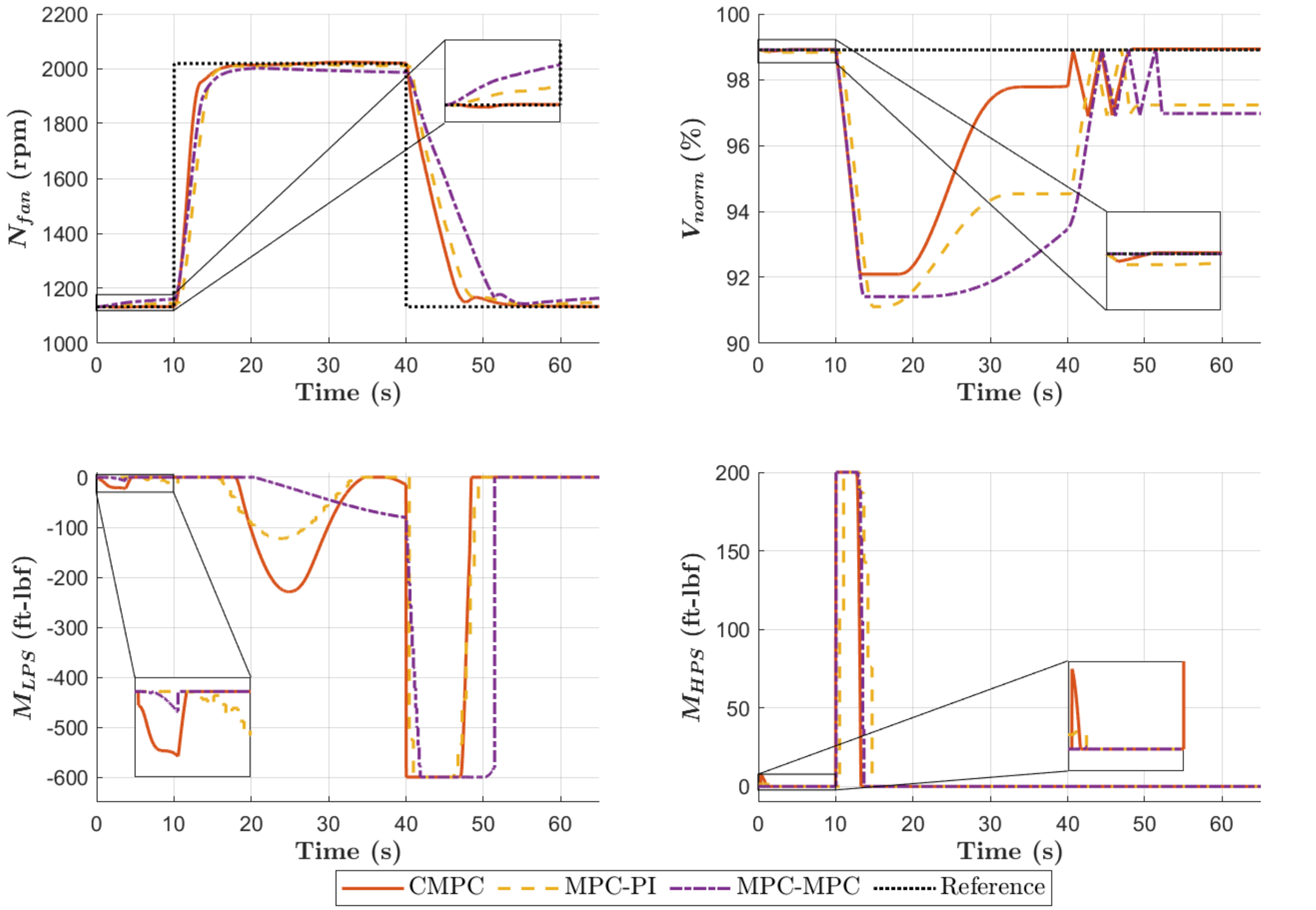

FIGURE 3: RESULTANT CLOSED-LOOP PERFORMANCE ACROSS CONTROLLERS FOR FAN SPEED (N_{fan}), NORMALIZED VOLTAGE OF THE SUPERCAPACITOR STATE-OF-CHARGE (V_{norm}), LPS EM MOTOR TORQUE (M_{LPS}), AND HPS EM MOTOR TORQUE (M_{HPS}).

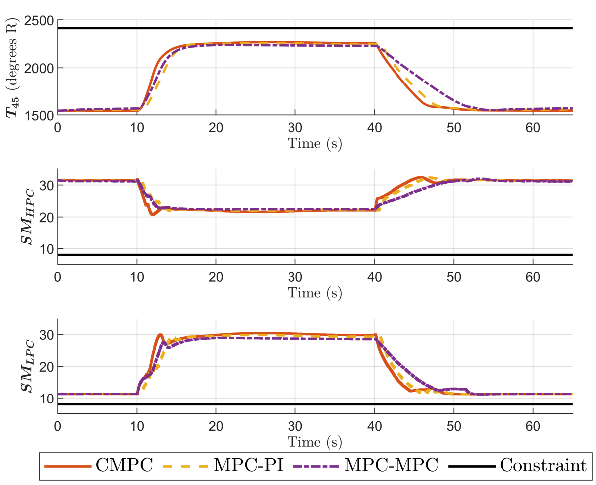

FIGURE 4: TEMPERATURE (T_{45}) AND HIGH/LOW COMPRESSOR STALL MARGIN (SM_{HPC}, SM_{LPC}) RESULTANT TRAJECTORIES.

relative to the CMPC data. In the cases of the HMPCs, the controller time was calculated as a sum of the C_{11} and C_{21} execution times. Simulations were executed on a laptop computer with an Intel® Core™ i7-118500H CPU @ 2.50GHz Processor. Computation times were computed with the Performance Advisor tool in Simulink. The data show that of the HMPCs, MPC-PI executes in the shortest amount of time, reducing total execution time and controller execution time by over 80% compared to the CMPC. Comparatively, using MPC-MPC results in only ~15% time reductions. HMPC execution times are heavily dependent on α, as this changes the sampling rate of the top-level MPC component of the architectures. As α approaches 1, the computation time lengthens, resulting in an execution time akin to the CMPC. The computational data highlight the advantage of HMPC schemes over non-HMPC architectures. By exploiting different sampling rates at each tier in the hierarchy, an HMPC can execute at a faster rate than a non-HMPC controller. In this case, both HMPCs exhibit execution time reductions to varying degrees. When taken in concert with the closed-loop performance, the outcomes emphasize the viability of HMPC as an alternative to non-HMPC controllers. These designs can be tuned to perform comparably

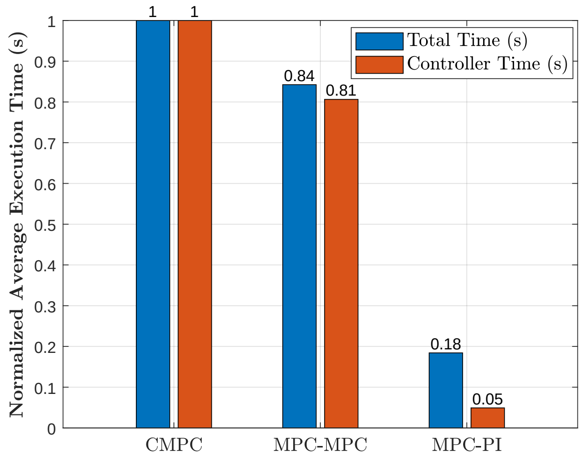

FIGURE 5: CONTROLLER EXECUTION TIMES WITH α = 10 FOR MPC-MPC AND α = 35 FOR MPC-PI.

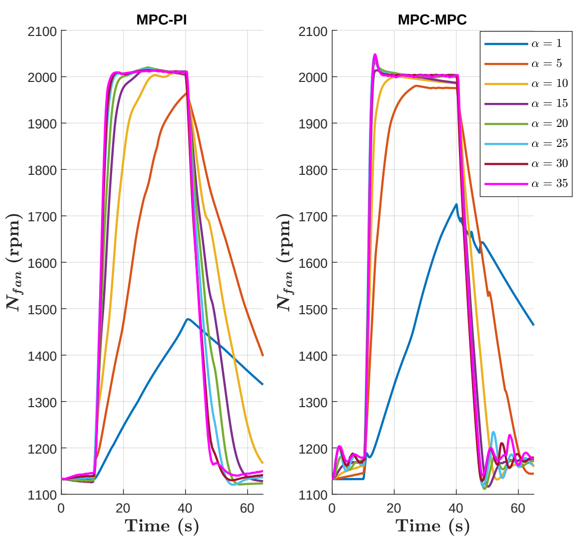

FIGURE 6: IMPACT OF SAMPLING TIME PARAMETER α ON HIERARCHICAL MPC SCHEMES.

and can be executed at faster speeds, thus combating the computational intensity pitfall of typical MPC schemes.

4.2 Effect of Sampling Time on HMPC

Sampling time plays a significant role in the design of MPCs, which are traditionally applied on slow dynamic systems. As such, the impact of the sampling time multiplier, α, on the closed-loop response of the HMPCs is evaluated. Neither HMPC was retuned for the evaluation but tuning over varying α profiles is a potential path for future research. Figure 6 shows the MPC-PI and MPC-MPC fan speed responses for values of α ranging from one to thirty-five. At $\alpha = 1$, both closed-loop responses exhibit the poorest tracking performance and at higher values of α, both HMPCs exhibit limited improvement in the response. As mentioned in Section 4.1, α contributes to steady-state error in the fan speed tracking response. This is clearly displayed in the figure, where both HMPCs have increasing levels of steady-state

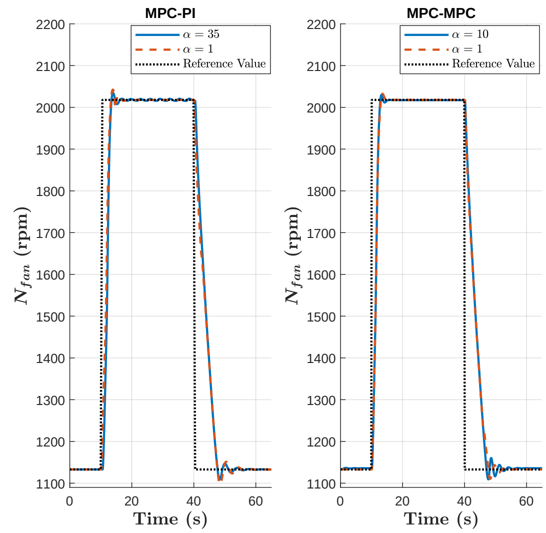

FIGURE 7: HIERARCHICAL MPCS IMPLEMENTED WITH TRUE REFERENCE VALUE, $N_{fan,ref}$, AT α = 1 AND TUNED α VALUES.

error prior to the burst and after the chop with change in the sampling time multiplier. For both controllers, as α increases, the acceleration response hastens, leading to significant overshoot at the largest α for MPC-MPC. In this controller, the deceleration response degrades, leading to varying levels of undershoot and steady-state error, the worst seeming to occur at $\alpha = 25$. Degradation is present, but not as severe, in the MPC-PI responses, where increasing α similarly quickens the rise response and impacts settling after the chop.

Investigation revealed that performance deterioration at $\alpha = 1$ is caused by the control design of C_{21}. In both HMPCs, C_{21} is tuned to respond to large error signals indicative of a step input, rather than small error signals indicative of a reference trajectory. At $\alpha = 1$, the optimal fan speed trajectory N^*_{fan} produced by C_{11} is a smooth trajectory profile whereas at larger α values N^*_{fan} mimics step-like behavior due to the sampling time discrepancy. This leads to the resultant trajectories observed in Fig. 6, where small sampling time multipliers inhibit the response and large sampling time multipliers improve the response. However, the performance discrepancy across α vanishes if the true fan reference value, $N_{fan,ref}$, is tracked by C_{21} in place of N^*_{fan}. Figure 7 demonstrates this behavior for both MPC-PI and MPC-MPC. Steady-state error, undershoot, and other poor performance characteristics are now absent due to tracking $N_{fan,ref}$. This outcome highlights the design considerations needed surrounding selection of the sampling time multiplier α and the tuning of lower tier controllers in the hierarchy. To achieve a desirable response via optimal setpoint tracking, α must be selected such that the sampling time of C_{11} is acceptably slower than that of C_{21}. Further, each α value necessitates retuning or redesign of C_{21} to best respond to reference trajectory, rather than reference point, tracking. Thus, as α has significant impact on the steady-state and transient characteristics of a response, it should be selected based on the dynamic needs of the system and the desired controller composition.

5. CONCLUSIONS

This paper presented two hierarchical MPC architectures for control of a hybrid-electric propulsion system. Both designs used a two-tier, one subsystem layout, combining a CMPC at the highest tier with either a CMPC or PI controller at the lowest tier. Case studies illustrated that the HMPCs maintained comparable closed-loop performance to CMPC, tracking fan speed and regulating energy storage devices, at reduced computational intensity. This outcome promotes HMPC as a feasible alternative to non-HMPC designs when computation time is a practical limitation. More importantly, the study revealed the sampling parameter α to warrant careful consideration in HMPC design. As shown in the case studies, α plays an influential role in the closed-loop performance of HMPC, emphasizing that its selection is critical in the design process. Potential directions for continued research have been highlighted in the case studies, but additional avenues include exploring multi-tier, multi-subsystem hierarchical architectures, incorporating additional MPC designs into HMPC, and implementing mission-preview with HMPC.

ACKNOWLEDGMENTS

Elyse Hill's research was supported by an appointment to the NASA Postdoctoral Program at the NASA Glenn Research Center, administered by Oak Ridge Associated Universities under contract with NASA. This work was also supported by funding from the Power and Propulsion subproject under the Advanced Air Transport Technology Project as a part of the NASA Advanced Air Vehicles Program.

REFERENCES

[1] Pearce, Bob. "NASA Aeronautics Strategic Implementation Plan 2023." (2023).

[2] Simon, Donald L., Thomas, Randy and Dunlap, Kyle M. "Considerations for the Extension of Gas Path Analysis to Electrified Aircraft Propulsion Systems." *Journal of Engineering for Gas Turbines and Power* Vol. 144 No. 3 (2021): p. 031004. DOI 10.1115/1.4052424. URL https://doi.org/10.1115/1.4052424.

[3] Simon, Donald L., Connolly, Joseph W. and Culley, Dennis E. "Control Technology Needs for Electrified Aircraft Propulsion Systems." *Journal of Engineering for Gas Turbines and Power* Vol. 142 No. 1 (2020): pp. 1–10. DOI 10.1115/1.4044969.

[4] Ma, Zhixun, Zhang, Xin, Huang, Jingjing and Zhao, Bin. "Stability-Constraining-Dichotomy-Solution-Based Model Predictive Control to Improve the Stability of Power Conversion System in the MEA." *IEEE Transactions on Industrial Electronics* Vol. 66 No. 7 (2019): pp. 5696–5706. DOI 10.1109/TIE.2018.2875418. URL https://ieeexplore.ieee.org/document/8493593.

[5] Kou, Peng, Wang, Jing and Liang, Deliang. "Powered Yaw Control for Distributed Electric Propulsion Aircraft: A Model Predictive Control Approach." *IEEE Transactions on Transportation Electrification* Vol. 7 No. 4 (2021): pp. 3006–3020. DOI 10.1109/TTE.2021.3068724. URL https://ieeexplore.ieee.org/document/9386122.

[6] Wang, Xin, Atkin, Jason, Bazmohammadi, Najmeh, Bozhko, Serhiy and Guerrero, Josep M. "Optimal Load and Energy Management of Aircraft Microgrids Using Multi-Objective Model Predictive Control." *Sustainability* Vol. 13 No. 24 (2021): p. 13907. DOI 10.3390/su132413907. URL https://www.mdpi.com/2071-1050/13/24/13907.

[7] Russo, Antonio, Canciello, Giacomo and Cavallo, Alberto. "MPC based Sliding Mode Control for More Electric Aircraft application." *2021 22nd IEEE International Conference on Industrial Technology (ICIT)*, Vol. 1: pp. 74–79. March 10–12, 2021. IEEE, Valencia, Spain. DOI 10.1109/ICIT46573.2021.9453663. URL https://ieeexplore.ieee.org/document/9453663.

[8] Almeida, Fabio. "Management of Electrical Power Generation on Gas Turbine with Model Predictive Control." *AIAA SciTech 2022 Forum*. AIAA 2022-0444: pp. 1–17. Jan 3–7, 2022. AIAA, San Diego, CA, USA. DOI 10.2514/6.2022-0444. URL https://arc.aiaa.org/doi/10.2514/6.2022-0444.

[9] Zhang, Jinning, Roumeliotis, Ioannis and Zolotas, Argyrios. "Nonlinear Model Predictive Control-Based Optimal Energy Management for Hybrid Electric Aircraft Considering Aerodynamics-Propulsion Coupling Effects." *IEEE Transactions on Transportation Electrification* Vol. 8 No. 2 (2022): pp. 2640–2653. DOI 10.1109/TTE.2021.3137260.

[10] Doff-Sotta, Martin, Cannon, Mark and Bacic, Marko. "Predictive Energy Management for Hybrid Electric Aircraft Propulsion Systems." *IEEE Transactions on Control Systems Technology* Vol. 31 No. 2 (2023): pp. 602–614. DOI 10.1109/TCST.2022.3193295. URL https://ieeexplore.ieee.org/document/9852004.

[11] Rawlings, James B. and Mayne, David Q. *Model Predictive Control: Theory and Design*, 2nd ed. Nob Hill Publishing, Madison (2009).

[12] Hill, Elyse, Amthor, Aria E., Soloway, Donald I., Simon, Donald L and Connolly, Joseph W. "Model Predictive Control Strategies for Turbine Electrified Energy Management." *Journal of Engineering for Gas Turbines and Power* (2023): pp. 1–24DOI 10.1115/1.4063783. URL https://doi.org/10.1115/1.4063783.

[13] Johansen, Tor A. "Toward Dependable Embedded Model Predictive Control." *IEEE Systems Journal* Vol. 11 No. 2 (2017): pp. 1208–1219. DOI 10.1109/JSYST.2014.2368129.

[14] Zhang, Jinning, Roumeliotis, Ioannis and Zolotas, Argyrios. "Sustainable Aviation Electrification: A Comprehensive Review of Electric Propulsion System Architectures, Energy Management, and Control." *Sustainability* Vol. 14 No. 10 (2022): p. 5880. DOI 10.3390/su14105880. URL https://www.mdpi.com/2071-1050/14/10/5880.

[15] Eren, Utku, Prach, Anna, Koçer, Başaran Bahadır, Raković, Saša V., Kayacan, Erdal and Açıkmeşe, Behçet. "Model Predictive Control in Aerospace Systems: Current State and Opportunities." *Journal of Guidance, Control, and Dynamics* Vol. 40 No. 7 (2017): pp. 1541–1566. DOI

10.2514/1.G002507. URL https://arc.aiaa.org/doi/10.2514/1.G002507.

[16] Alleyne, Andrew G. and Aksland, Christopher T. "Control as an Enabler for Electrified Mobility." *Annual Review of Control, Robotics, and Autonomous Systems* Vol. 5 No. 1 (2022): pp. 659–688. DOI 10.1146/annurev-control-042920-012513. URL https://www.annualreviews.org/doi/10.1146/annurev-control-042920-012513.

[17] Koeln, Justin P., Pangborn, Herschel C., Williams, Matthew A., Kawamura, Malia L. and Alleyne, Andrew G. "Hierarchical Control of Aircraft Electro-Thermal Systems." *IEEE Transactions on Control Systems Technology* Vol. 28 No. 4 (2020): pp. 1218–1232. DOI 10.1109/TCST.2019.2905221. URL https://ieeexplore.ieee.org/document/8689055.

[18] Wang, Wenqing and Koeln, Justin P. "Hierarchical Multi-Timescale Energy Management for Hybrid-Electric Aircraft." *ASME 2020 Dynamic Systems and Control Conference*: p. V001T11A002. Oct 5–7, 2020. Virtual, Online. DOI 10.1115/DSCC2020-3190. URL https://asmedigitalcollection.asme.org/DSCC/proceedings-abstract/DSCC2020/84270/V001T11A002/1096476.

[19] Aksland, Christopher T. and Alleyne, Andrew G. "Experimental Model and Controller Validation for a Series Hybrid Unmanned Aerial Vehicle." *2020 American Control Conference (ACC)*: pp. 4154–4160. 2020. IEEE, Denver, CO, USA. DOI 10.23919/ACC45564.2020.9147529. URL https://ieeexplore.ieee.org/document/9147529.

[20] Aksland, Christopher T. and Alleyne, Andrew G. "Hierarchical model-based predictive controller for a hybrid UAV powertrain." *Control Engineering Practice* Vol. 115 (2021): p. 104883. DOI 10.1016/j.conengprac.2021.104883. URL https://www.sciencedirect.com/science/article/pii/S096706612100160X.

[21] Aksland, Christopher T., Tannous, Pamela J., Wagenmaker, Minda J., Pangborn, Herschel C. and Alleyne, Andrew G. "Hierarchical Predictive Control of an Unmanned Aerial Vehicle Integrated Power, Propulsion, and Thermal Management System." *IEEE Transactions on Control Systems Technology* Vol. 31 No. 3 (2023): pp. 1280–1295. DOI 10.1109/TCST.2022.3220913. URL https://ieeexplore.ieee.org/document/9960782.

[22] Chapman, Jeffryes W. and Litt, Jonathan S. "Control Design for an Advanced Geared Turbofan Engine." *53rd AIAA/SAE/ASEE Joint Propulsion Conference*. AIAA 2017-4820. Atlanta, GA, USA, July 10–12, 2017. DOI 10.2514/6.2017-4820. URL https://arc.aiaa.org/doi/10.2514/6.2017-4820.

[23] Chapman, Jeffryes W., Lavelle, Thomas M., May, Ryan D., Litt, Jonathan S. and Guo, Ten-Huei. "Toolbox for the Modeling and Analysis of Thermodynamic Systems (T-MATS) User's Guide." Technical Report No. NASA/TM-2014-216638. NASA, Cleveland, OH. 2014. URL https://ntrs.nasa.gov/citations/20140012486.

[24] Chapman, Jeffryes W. and Litt, Jonathan S. "An Approach for Utilizing Power Flow Modeling for Simulations of Hybrid Electric Propulsion Systems." *2018 AIAA/IEEE Electric Aircraft Technologies Symposium (EATS)*. AIAA 2018-5018. Cincinnati, OH, July 9–11, 2018. DOI 10.2514/6.2018-5018. URL https://doi.org/10.2514/6.2018-5018.

[25] Culley, Dennis E., Kratz, Jonathan L. and Thomas, George L. "Turbine Electrified Energy Management (TEEM) For Enabling More Efficient Engine Designs." *2018 Joint Propulsion Conference*. AIAA 2018-4798. Cincinnati, OH, July 9–11, 2018. DOI 10.2514/6.2018-4798. URL https://doi.org/10.2514/6.2018-4798.

[26] Kratz, Jonathan L., Culley, Dennis E. and Thomas, George L. "A Control Strategy for Turbine Electrified Energy Management." *AIAA Propulsion and Energy 2019 Forum*. AIAA 2019-4499. Indianapolis, IN, August 19–22, 2019. DOI 10.2514/6.2019-4499. URL https://doi.org/10.2514/6.2019-4499.

[27] Andersson, Joel A. E., Gillis, Joris, Horn, Greg, Rawlings, James B. and Diehl, Moritz. "CasADi: a software framework for nonlinear optimization and optimal control." *Mathematical Programming Computation* Vol. 11 No. 1 (2019): pp. 1–36. DOI 10.1007/s12532-018-0139-4.